Title

Intrinsic rotation reversal, non-local transport, and turbulence transition in KSTAR L-mode plasmas

Journal

Nuclear Fusion, 57(6)

ISSN

0029-5515

Authors

Shi, YJ
Kwon, JM
Diamond, PH
et al.

Publication Date

2017-06-01

DOI

10.1088/1741-4326/aa6b23

Intrinsic rotation reversal, non-local transport, and turbulence transition in KSTAR L-mode plasmas

Y.J.Shi[1], J.M. Kwon[2], P.H.Diamond[3], W.H.Ko[2], M.J.Choi[2], S.H.Ko[2], S.H.Hahn[2], D.H.Na[1], J.E.Leem[4], J.A.Lee[4], S.M.Yang[1], K.D.Lee[2], M.Joung[2], J.H.Jeong[2], J.W.Yoo[2], W.C.Lee[2], J.H.Lee[2], Y.S.Bae[2], S.G.Lee[2], S.W.Yoon[2], K. Ida[5] , and Y-S.Na[1]

[1]Department of Nuclear Engineering, Seoul National University, Seoul, Korea
[2]National Fusion Research Institute, Daejeon, Korea
[3]CMTFO and CASS, University of California, San Diego, USA
[4]Pohang University of Science and Technology, Pohang, Korea
[5]National Institute of Fusion Science, Toki, Japan
E-mail contact of main author: yjshi@snu.ac.kr yjshi@ipp.ac.cn

Abstract. Experiments of electron cyclotron resonance heating (ECH) power scan in KSTAR tokamak clearly demonstrate that both the cutoff density for non-local heat transport (NLT) and the threshold density for intrinsic rotation reversal can be determined by the collisionality. We demonstrate that NLT can be affected by ECH, and the intrinsic rotation direction follows the changes of NLT. The cutoff density of NLT and threshold density for rotation reversal can be significantly increased by ECH. The poloidal flow of turbulence in core plasma is in the electron and the ion diamagnetic direction in ECH plasmas and high density OH plasma, respectively. The auto-power spectra of density fluctuation are almost the same in the outer region for both ECH and OH plasmas. On the other hand, the divergence in density fluctuation spectra at high frequency range between OH and ECH plasma is clearly observed in core region. The features of linear confinement and saturated confinement are also appeared in ECH plasma, which is similar to the linear ohmic confinement (LOC) mode and saturate ohmic confinement. (SOC) mode. All these observations in macroscopic parameters and micro fluctuations suggest a possible link between the macro phenomena and the structural changes in turbulence mode.

1. Introduction

There are several outstanding experimental mysteries in magnetic fusion plasma research. A rapid increase of the central electron temperature caused by the edge cooling in Ohmic plasmas, the so called non-local transport (NLT) [1] is one of these issues. Although NLT was observed in the TEXT tokamak 21 years ago, and in many fusion devices afterwards [2-11], the underlying physics mechanism is still unclear. One typical characteristic of NLT is this effect disappears with increasing electron density. The critical density where the NLT effect disappears is defined as cutoff density. On the other hand, the reversal of the intrinsic plasma rotation found recently [12-16] is another mystery in tokamak plasma transport. Similar to NLT events, the intrinsic rotation reversal in ohmic heating (OH) plasma is also related to a threshold density. The toroidal rotation at the center of the plasma reverses its direction when

the plasma density exceeds certain level in density ramping-up OH plasma experiments [13-16]. Intrinsic rotation is particularly important for International Thermonuclear Experimental Reactor (ITER), since neutral beam injection (NBI) is not sufficient to drive the requisite rotation on ITER and future reactors. It is still challenging to understand heat transport fully and origin of intrinsic rotation in magnetic fusion plasma, which is very important for predictions of the performance of burning plasma tokamaks like ITER.

In the latest KSTAR experiment, we found that the cutoff density of NLT can be significantly increased by applying ECH. At the same time, the threshold density of core intrinsic rotation reversal is also increased with ECH. The increment of cutoff density for NLT or intrinsic rotation reversal is proportional to the injecting power of ECH. KSTAR's ECH experiments in this paper show the close correlation between NLT and intrinsic rotation reversal. On the other hand, the microscope measurement results show that the density fluctuation of ECH plasma is stronger than OH plasma in core region while it is almost same for OH and ECH plasma in outer region. Moreover, in the core region, the measured turbulent poloidal flow of ECH plasma is in electron diamagnetic direction electron while it changes to ion diamagnetic direction in high density OH plasma. The turbulent poloidal rotation reversal (electron direction in ECH plasma, ion direction in high density OH plasma), which is found for the first time in KSTAR, is the powerful experimental indicator for the turbulence transition between electron mode and ion mode. We try to elucidate possible physics mechanism for NLT and rotational reversal from both the experimental results and gyro-kinetic stability analysis.

This paper is organized as follows: first, an introduction to the experiment setup in KSTAR is given in section 2, which includes heating schemes and diagnostics, and relevant plasma parameters. The main experimental results are described in section 3. Discussions on possible physical mechanisms for the intrinsic rotation behavior and non-local transport are presented in section 4. Gyro-kinetic analysis of micro-stability is given in section 5. Summary and future plan are presented in section 6.

2. Experimental setup

All the results presented in this paper were obtained in KSTAR superconducting tokamak [17]. Charge exchange recombination spectroscopy (CES) [18] is one of main diagnostics for the measurement of temperature (T_i) and toroidal rotation velocity (V_ϕ) of carbon impurity ions. The system has 32 toroidal lines of sight and can provide complete plasma profiles from

the plasma edge to the magnetic axis. The x-ray imaging crystal spectrometer (XICS) [19] in KSTAR also can provide one channel data of T_i and V_ϕ for core plasma. Electron temperature was measured with the electron cyclotron emission radiometer (ECE) [20]. The line averaged density measurements are based on microwave interferometry. Thomson scattering [21] provided localized density information for some shots in this paper. Moreover, the electron cyclotron emission imaging system (ECEI) [22] can provide the information of temperature fluctuation. Microwave imaging reflectometry (MIR) [23] measure the density fluctuation in KSTAR.

Neutral beam injection (NBI) beam blip is used for the measurement of CES. Multi-pulse supersonic molecular beam injection (SMBI) [24] is applied to trigger NLT and find the cutoff density. Simple structure, good flexibility and relatively high fuelling efficiency make SMBI the most suitable tool to investigate NLT phenomenon which has been firstly applied to fusion plasma in HL-1M tokamak [25]. There are three ECH heating systems in KSTAR [26]. One is 110 GHz (source power of 0.5 MW) and the others are 170 GHz (source power of 1 MW) and 140/105 GHz (source power of 1.0 MW with dual frequency). The experimental data in this paper was obtained with the 170 or 140 GHz ECH heating system. The ECH system was configured for an X-mode second harmonic and the deposition location was on-axis position.

The main plasma parameters in this experiment are I_p = 0.5 MA, B_T = 2.9 T for 170 GHz ECH and 2.5 T for 140 GHz ECH. Discharges were operated in elongated limiter configurations. Plasma elongation and the edge safety factor are κ = 1.35-1.45, q_{95} = 6.7-7.1 and κ = 1.61-1.65, q_{95} = 7.2-7.5 for B_T = 2.9 T and B_T = 2.5 T, respectively.

3. Experimental results

In 2015 KSTAR experiment, we found that the cutoff density of NLT can be significantly increased by applying 170 GHz ECH at B_T = 2.9T. Fig.1 shows the waveforms of a representative ECH discharge and OH discharge in KSTAR. The two shots in fig.1 have the same plasma operation parameters such as plasma current and magnetic field. The difference between the two shots results from the injection of 700kW on-axis ECH at the current flattop phase in one discharge. It is clear that the NLT effect (core T_e rise while edge T_e drops) appears in the first SMBI pulse and gradually weakens in later SMBI pulses with increasing density in ECH plasma. Still, very weak NLT can be observed in the last SMBI pulse at $\bar{n}_e$ =

$2.4\times10^{19}m^{-3}$ in this ECH plasma. On the other hand, NLT cannot be trigged by the first SMBI pulse even at relatively low density of $\bar{n}_e$ = $1.5\times10^{19}m^{-3}$ in the OH plasma (the blue curves in fig.1). Due to limited machine time, we couldn't measure the exact cutoff density for the OH plasma in 2015 KSTAR campaign.

Fig. 2 shows the detailed time trace of T_e at different radii for one typical NLT event in the ECH plasma. The response of T_e rise in the core is about 16ms delayed after the T_e drop at the edge, which is much shorter than the energy confinement time (~100ms) for this plasma. Although sawtooth instabilities appear in this discharge, the NLT-induced core T_e increase shows a longer time scale than the sawtooth time scale, and the sawtooth activities do not change the overall NLT trends.

Fig.3 shows the 2-D electron temperature images taken from ECEI during NLT in the ECH plasma shown in in fig.1 and fig.2. Compared to the 1-D ECE signals shown in fig.2, ECEI images can show more intuitional and clearer structures in 2-D space during NLT. The big red spot represents the area with T_e increase during NLT. Here, we call this red spot as the NLT pattern. At the same time, m/n = 1 island, the small blue spot around the q = 1 surface, is also clearly seen inside the NLT pattern, which corresponds to the sawtooth activities identified in the ECE signals (see fig.2). We note that there is no other obvious island structure observed other than this m/n = 1 island. The m/n = 1 island rotates while the whole NLT pattern does not rotate in the time period shown in fig.3. Both the ECEI images in fig.3 and ECE signals in fig.2 indicate that the correlation between the NLT and the sawtooth activity is weak.

In addition to the NLT event, we found another macroscopic difference in the ECH and the OH plasmas. Fig.4 compares the equilibrium profiles of the ECH and OH plasmas presented in fig.1 at same density level ($\bar{n}_e = 2.0 \times 10^{19} m^{-3}$.). It is well known that ECH provides localized electron heating. As a result, the increase of electron temperature and its gradient in the center is observed as expected in such on-axis ECH case (see fig.4a and fig.4d). On the other hand, the increment of ion temperature by ECH is only about 10% in whole region. The gradient of T_i show little change. One notable point in fig.4c is the core toroidal rotation, which is in the counter-current direction in the OH plasma whereas the co-current direction in ECH plasma. As observed in previous experiments, the intrinsic rotation reversal in OH plasma is normally achieved by increasing the electron density [13-16]. However, here we use the ECH to achieve a very similar phenomenon of intrinsic rotation reversal, as reported in the literature [13-16]. Rotation reversals by ECH in H-mode plasmas are also reported in DIII-D

[27]. In KSTAR, ECH H-mode plasma is hoped to be achieved with more Gyrotrons and higher ECH power at same working frequency in the future.

We tried to repeat the similar experiment in 2016 KSTAR campaign, but using the new 140GHz ECH system with B_T = 2.5T. The same trend of NLT has been found with this experimental condition but increment of cutoff density for NLT and the threshold density for rotation reversal is newly found to be proportional to the ECH power as shown in fig.5. The cutoff density is only 1.21~1.25×$10^{19}$$m^{-3}$ for the OH plasma, but it is dramatically increased to 2.2~2.3 ×10^{19} m^{-3} in 800 kW ECH plasma. On the other hand, the normalized effective collisionality (ν_{eff}) at half normalized radius (ρ~0.5) at cutoff density is almost the same for the four OH and ECH shots. The ν_{eff} is the collision frequency normalized by drift frequency [28]

$$\nu_{eff} = \frac{\nu_{ei}}{\omega_{DE}} \approx 0.1 n_e Z_{eff} \frac{R}{T_e^2}$$

where n_e is the electron density in , Z_{eff} is the effective in charge, R is the major radius in m and T_e is the electron temperature in keV.

The time evolution of the core toroidal rotation is shown in fig.6. The data in fig.5 and fig.6 were obtained from the same discharges. ECH is injected from 3s to 7s for three ECH shots. For the OH shot 16471, the core V_ϕ is in the co-current direction in the initial low density phase, and gradually decreases and changes to the counter-current direction as the density increases. For the three ECH shots, there appear very clear increments of the core V_ϕ in the co-current direction as ECH is injected. However, very interestingly, the core V_ϕ decreases as the density reaches a certain level in the ECH plasmas. Although the absolute value and the ramp-up rate of density are almost identical for the three ECH shots, the threshold density for the core V_ϕ reversal (co-direction→ counter-direction) is obviously higher for higher ECH power heating. The modulation frequency of NBI blips is 2Hz. So the exact timing of the core rotation reversal is hard to identify in these plasmas. But we can estimate the threshold density for the rotation reversal from the time evolutions. The estimated threshold density, which is also shown in fig.5, is very similar to the cutoff density for NLT in fig.5. More important finding is that both the cutoff density for NLT and the threshold density for the rotation reversal increase as the ECH power increases. And ν_{eff} at rotation reversal point is also quite close to the ν_{eff} at cutoff point. On the other hand, the maximum value of core $V\phi$ shows little changes for the ECH power variation.

The fluctuation characteristics of these ECH and OH plasmas are also investigated by 2-D MIR fluctuation diagnostics. Fig.7 shows the density fluctuation measured with the MIR system. It can be seen that the auto-power spectra of density fluctuations are almost the same for both the ECH and OH plasma in the outer region ($\rho>0.4$). However, in the core region ($\rho<0.3$), the divergence between ECH and OH is quite clear. The discrepancy in the density power spectra between the ECH and the OH plasma increases with the frequency, especially at the relative high frequency range. The wave number estimated with the method in [29] is also plotted in fig.7. Although trapped electron mode (TEM) mode and ion temperature gradient (ITG) are overlapped in the domain of $k_\theta\rho_s<1$, higher $k_\theta\rho_s$ should be corresponded to more electron scale turbulence. The enhanced fluctuation intensity of ECH plasma at high frequency (i.e high wave number) in fig.7a implies stronger turbulence activity in electron mode.

MIR can also provide the information of poloidal rotation velocity V_θ [23, 30]. Fig.8 shows the cross-phase spectra of MIR in the core region at a low density ECH phase and a high density OH phase. V_θ estimated from the dispersion relation of cross-phase spectrum is about 6.5km/s in the electron diamagnetic direction in the ECH phase and 7km/s in the ion diamagnetic direction in the OH phase. According to Ref.23 and 30, the apparent poloidal rotation velocity measured by MIR also includes the contribution from toroidal flow. Here, the effects of V_ϕ to V_θ can be excluded. Firstly, V_ϕ in non-NBI heating plasma in this paper is much smaller than that in NBI heating plasma in Ref.23 and 30. Secondly, the toroidal flow in the core region is co-current direction in the ECH plasma and counter-current direction in high density OH plasma as shown in previous part. Contribution from toroidal flow is in the ion diamagnetic direction for co-current toroidal rotation and in the electron diamagnetic direction for counter-current toroidal rotation. Moreover, static poloidal rotation velocity estimated with neoclassic calculation [31] is only about 1km/s in the core region for the plasma parameters presented in this paper. So, here, the apparent V_θ mainly represents the phase velocity of turbulence. Now, the microscopic poloidal rotation reversal of turbulence (electron diamagnetic direction in the ECH plasma, ion diamagnetic in the high density OH plasma) is disclosed for the first time, which is covered by the more obvious macroscopic toroidal flow reversal (co-current in the ECH plasma and counter-current in the high density OH plasma).

4. Discussion on physical mechanisms for intrinsic rotation reversal and non-local transport

The experimental observations in the previous section suggest a possible link between the macro phenomena and the structural changes in micro-fluctuations. One prominent theoretical hypothesis to explain the cutoff density for NLT is the transition of dominant fluctuation mode from trapped electron mode (TEM) mode to ion temperature gradient (ITG) related to the confinement regime transition between linear ohmic confinement (LOC) and saturated Ohmic confinement (SOC) [32-34]. Turbulence is triggered by cold pulse in the outer unstable LOC plasma and propagates to the core with very fast spreading process. The core part of LOC plasma is below marginal stability and provides room for further performance improvement until the SOC is reached. The gap of density fluctuation spectrum between OH and ECH plasma in fig.7 indicates such rooms to increase performance. So the transition point for LOC-SOC is the responsible for the cutoff density of NLT. It is known that the collisionality is one key issue to determine the dominated turbulence mode or confinement status. Fig.5 shows that the normalized effective collisionality at higher density with higher ECH power is the same level as the low density OH plasma. The relation between global confinement time (τ_E) and line average density is also shown in fig.9. The range of LOC and SOC of OH plasma is marked out with the yellow line in fig.9. Although τ_E of ECH plasma is only 1/3~1/2 of OH plasma, the linear confinement region and saturated confinement region, which are labeled with green line, are also existed in ECH plasma. The transition density between linear confinement region and saturated region in ECH plasma is much higher than that for LOC-SOC in OH plasma, which is consistent the increasing trend of cutoff density of NLT by ECH.

On the other hand, the intrinsic rotation reversal can also be explained by the transition of the fluctuation or confinement mode [35-36]. Due to the excellent localized heating, ECH is a good control ‘knob’ for the micro-turbulence population. Although the toroidal rotation driven by ion cyclotron resonance heating (ICRF) and lower hybrid current drive (LHCD) has also been observe in many devices, the mechanism for torque or rotation change induced by ECH is not exactly the same as ICRF or LHCD plasma. ICRF can directly drive toroidal flow with mode conversion [37] or energetic particles accelerated by wave [38]. LHCD-driven rotation is also affected by many actuators which include fast electron ripple loss effects, thermal ripple induced neoclassical friction, and direct LH wave effects [39-40]. ECH almost

does not bring such complicated factor as ICRF or LHCD. The extremely low toroidal field ripple in KSTAR (as low as ~ 0.05% [41]) can also further reduce the effect of fast particle ripple loss and the ripple induced neoclassical friction for thermal particle. On the whole, the rotation change by ECH in KSTAR is more likely related to the variation of turbulence induced intrinsic torque.

The relation between the cutoff density for NLT (or threshold density for rotation reversal) and the ECH power strongly implies that the transition or change of micro-turbulence mode is a possible cause for the rotation reversal or the cutoff density for NLT. But there are still several puzzles in the detailed physical processes for the formation of intrinsic toroidal rotation profile. The first is why the core rotation direction flips only, while the edge rotation still in the co-current direction? The second one is why the co-directional core rotation profile in the low density OH plasma has a flatter form than the counter-directional rotation profile in the high density OH plasma. These two characters of the rotation profiles are also observed in fig.4c in this paper. Here, we provide a possible explanation for these puzzles. As shown in fig.10, we consider there are two types of intrinsic torque. The first one is an edge/SOL intrinsic torque, which depends on plasma boundary and SOL conditions. The second torque is located in core plasma and driven by turbulence. The direction of the second torque can be reversed, if the dominant turbulence mode is changed from ITG to TEM or TEM to ITG. We want to emphasize that the direction of ITG/TEM-driven torque is not fixed, and depends on other plasma parameters such as the magnetic shear or plasma current profile [42, 43]. For example, TEM-driven torque can be in counter-direction for plasma with flat or reversal current profiles and in co-current direction with monotonic current profiles [42, 43]. For the OH and ECH plasmas with peaked monotonic current profile, ITG/TEM-driven torque can be in counter/co direction. In high density OH plasmas, the very similar intensity of density fluctuation for OH and ECH plasmas in fig.7d indicts that TEM is still the dominant turbulence mode in outer region of OH plasma. On the other hand, the divergence of fluctuation spectrum between OH and ECH in fig.7a and the turbulence propagation in ion direction in fig.8a suggest that the ITG maybe the main turbulence mode the in core region for high density OH plasma. The combined actions of the counter-direction ITG-driven torque in core plasma, co-direction TEM-driven torque in outer region and co-direction torque in edge/SOL region can make the reversal happen only in the core.

In low density OH or ECH plasmas, on the other hand, the rotation is in co-direction in the whole region and the rotation profile is nearly flat in the core. There is no doubt that worse

confinement in low density OH or ECH plasmas is one contributor for the formation of flat profile. Here, we note that the neoclassical toroidal viscosity (NTV) due to MHD activity [44, 45] can be a damping mechanism. Although, TEM intensity can be enhanced with high electron temperature and its gradient, MHD activities also increase as the electron temperature and its gradient increase. Fig.11 shows the fluctuation power spectrum of T_e ($\delta T_e/T_e$) measured by ECE at ρ~0.5. The fluctuation of T_e in low frequency domain can represent the intensity of MHD activity. It can been seen that the fluctuations of T_e for low density OH plasma (green line in fig.11) is stronger than that of high density OH plasma (brown line in fig.11), which implies that the MHD-induced damping can be bigger in the low density OH plasma and make the core rotation profile more flat. Fig.11 also implies that the MHD damping can increase with the power of ECH. This may explain why the maximum co-rotation value does not increase with the ECH power. The electron temperature gradient mode (ETG) is the other possibility for the saturated maximum co-rotation of ECH plasma. The ion response to the ETG with high wave numbers is adiabatic. Little momentum transport or residual stress in ion channel will be affected by those small scale ETGs. At present, KSTAR's MIR can only provide the turbulence information up to $k_\theta\rho_s$~1. We will get convinced experimental ETG proof if KSTAR will install high k diagnostics in future.

Two experimental evidences to support TEM-driven co-direction torque are shown in fig.12 and 13. Fig.12 shows the evolutions of the rotation profile in during one discharge (shot16475). For the low density ECH plasma, the core rotation reaches a high level (~20km/s). Moreover, the clear gradient of V_ϕ (peaked profile) appears in the core region in the low density ECH plasma. One the other hand, the V_ϕ profiles of low density OH plasma and high density ECH plasma is quite flat in core. The core V_ϕ of high density OH plasma change to counter-current direction and is hollow, which may be caused by ITG driven toque. Fig.13 shows the continuous time evolution of the core V_ϕ measured by XICS. The parameters for the shot 16478 in fig.13 are almost identical with the shot 16475 in fig.12 except NBI beam blips. It can be seen that there is a prompt change of the core V_ϕ after the ECH injection. Then there is a slowly increasing phase of the V_ϕ. The prompt change of the core V_ϕ, which is corresponded to the fast drop phase of ν_{eff} after ECH injection, is much faster than the typical momentum confinement time of about hundred milliseconds in KSTAR and should be induced by the enhanced co-direction TEM-driven torque by ECH. The profiles of edge electron temperatures in this shot are shown in fig.14. Both the amplitude and gradient of edge T_e increase quite a lot after ECH injection, which may provide higher edge

torque for ECH plasma. The slower change of V_ϕ in fig.13 can be caused by the enhanced edge/SOL torque through transport mechanisms such as the momentum pinch, which is very similar to the phenomenon in Ref [46].

5. Gyro-kinetic linear stability analysis

To investigate the possible change of the turbulence characteristics, numerical studies have been performed for the OH and ECH plasmas using the gyro-kinetic code GYRO [47, 48]. Linear gyro-kinetic simulations have been conducted at the radii from ρ= 0.25 to ρ= 0.55. These results are presented in fig.15 where the positive and the negative mode frequencies imply the modes propagate in the electron and the ion diamagnetic drift direction, respectively. It can be seen that the TEM is dominant for the whole simulated region in the ECH plasma. At the outer region (ρ= 0.55) both the mode frequency and the growth rate are very similar between the OH plasma and the ECH plasma. In the core region, the divergence of growth rate between OH and ECH plasma become larger as the radial location moves to the center, which is consistent with experimental density fluctuation spectrum in fig.7. Especially, at the deep core region (ρ= 0.25), there is no linearly excited mode in the OH plasma while strong TEM still exist in the ECH plasma. At the same time, GRYO results show that the mode frequency of the OH plasma is always in electron side, which is not coincide with measured results of turbulence propagation in ion direction for OH core plasma in fig.8. On the other hand, the reduction of mode frequency for OH plasma at ρ= 0.35 is clearly towards the ion direction. The change of mode frequency to lower values towards ion direction indicates that the transition from TEM to ITG may be within the error bars. More detail improved simulation with sensitivity scan of the experimental data with error bars will be performed in future work.

6. Summary and future plans

In summary, the correlation between non-locality transport events and rotation reversals has been found in KSTAR L-mode plasmas. The cutoff density for non-locality transport can be increased by ECH heating. The toroidal rotation for the core plasma is reversed from the counter-current direction in the OH plasma to the co-current direction in the ECH plasma. Both the cutoff density for NLT and the threshold density for the core rotation reversal increase with the power of ECH. ECEI image indicates that the NLT phenomenon has weak relation to sawtooth activity. Moreover, the experimental results of ECH power scan indicate

that the collisionality is the key parameter to determine these critical densities. The characteristic of linear confinement and saturated confinement for ECH plasma, which is similar to LOC and SOC of OH plasma, is also found. The transition density in ECH plasma from linear to saturated confinement is much higher than the density for LOC-SOC transition. These correlated macro phenomenon, which is consistent with the hypothesis of turbulence theory to a great extent, indicate that the transition of dominant turbulence mode between TEM to ITG is the underline mechanism. The microscopic turbulent poloidal rotation reversal (electron diamagnetic direction in ECH plasma, ion diamagnetic in high density OH plasma), which is found for the first time in KSTAR, is the powerful experimental evidence for the turbulence mode transition (ITG↔TEM). The KSTAR experimental results seem to suggest that the intrinsic toroidal rotation profiles in OH/ECH plasmas are determined by the interplay of (i) an edge/SOL intrinsic torque, which is in co-current direction, (ii) a core intrinsic torque, which is in counter-current direction for high density SOC plasma and co-direction for low density LOC and ECH plasmas, (iii) MHD-induced damping. The linear instability study also shows that strong TEM instabilities are excited in the deep core region of the ECH plasmas. The increase of the electron temperature by ECH can reduce the collisionality for a given density, which impacts the destabilization of TEM. Also, the steepening of T_e gradient can help the excitation of TEM. The divergence of growth rate between OH and ECH plasmas in core region from numerical gyrokinetic simulation consists with the observed gab in density fluctuation spectrum measured with MIR. On the other hand, GYRO results do not show clear ITG↔TEM transition. Improved simulation with sensitivity analyses with the consideration of error bars for experimental data will be done in the future. Nonlinear gyro-kinetic simulations are also necessary to address more quantitative aspects of turbulence change and its effects on intrinsic torque and global profiles, which will also be performed in next step.

Acknowledgement

Yuejiang Shi is grateful to Dr. Hogun Jhang of National Fusion Research Institute (NFRI) in Korea who pointed out the possible increase of transition density for linear to saturated confinement regime in ECH plasma. Dr. Shi also thanks Dr. Hyunseok Kim of NFRI who provided the important data of energy confinement time. This research was supported by the R&D Programs through National Research Foundation of Korea (NRF) funded by the Ministry of Science, ICT and Future Planning of the Republic of Korea (No. 2014M1A7A1A03045368). This work is also supported by the R&D Programs through NFRI funded by the Ministry of Science, ICT and Future Planning of the Republic of Korea (NFRI-EN1741-3).

Reference

[1] Gentle K. *et al* 1995 *Phys. Rev. Lett.* **74** 3620

[2] Kissick M. *et al* 1996 *Nucl. Fusion* **36** 1691

[3] Mantica P. *et al* 1999 *Phys. Rev. Lett.* **82** 5048

[4] Ryter F. *et al* 2000 *Nucl. Fusion* **40** 1917

[5] Zou X. *et al* 2000 *Plasma Phys. Control. Fusion* **42** 1067

[6] Mantica P. *et al* 2002 *Plasma Phys. Control. Fusion* **44** 2185

[7] Tamura N. *et al* 2005 *Phys. Plasmas* **12** 110705

[8] Sun H.J. *et al* 2010 *Plasma Phys. Control. Fusion* **52** 045003

[9] Rice J. *et al* 2013 *Nucl. Fusion* **53** 033004

[10] Gao C. *et al* 2014 *Nucl. Fusion* **54** 083025

[11] Ida K. *et al* 2015 *Nucl. Fusion* **55** 013022

[12] Ida K. *et al* 2001 *Phys. Rev. Lett*. **86** 3040

[13] Bortolon A. *et al* 2006 *Phys. Rev. Lett*. **97** 235003

[14] Rice J. *et al* 2011 *Phys. Rev. Lett*. **107** 265001

[15] Angioni C. *et al* 2011 *Phy. Rev. Lett* **107** 215003

[16] Na D.H. *et al* 2016 *Nucl. Fusion* **56** 036011

[17] Lee G.S. *et al* 2000 *Nucl. Fusion* **40** 575

[18] Ko W.H. *et al* 2010 *Rev. Sci. Instrum.* **81** 10D740

[19] Lee S.G. *et al* 2010 *Rev. Sci. Instrum.* **81** 10E506

[20] Jeong S.H. *et al* 2010 *Rev. Sci. Instrum*. **81** 10D922

[21] Lee J.H. *et al* 2010 *Rev. Sci. Instrum*. **81** 10D528

[22] Yun G.S. *et al* 2010 *Rev.Sci.Instrum*. **81** 10D930

[23] Lee W.C. *et al* 2014 *Nucl. Fusion* **54** 023012

[24] Kim Y. O. *et al* 2012 *Fusion Eng. Design* **88** 1132

[25] Yao L. H. *et al* 1998 *Nucl. Fusion* **38** 631

[26] Bae Y.S. *et al* 2014 *Fusion Sci. Technol*. **65** 88

[27] deGrassie J. S. *et al* 2007 *Phys. Plasmas* **14** 056115

[28] Peeters A.G. *et al* 2005 *Nucl. Fusion* **45** 1140

[29] Bravenec R.V. and Wootton A.J. 1995 *Rev.Sci.Instrum*. **66** 802

[30] Lee W. C. *et al* 2016 *Phys. Plasmas* **23** 052510

[31] Kim Y. B. *et al* 1991 *Phys. Fluids* B **3** 2050

[32] Diamond P.H. *et al* 2008 *Phys. Plasmas* **15** 012303

[33] Naulin V. *et al* Rotation reversal in a 1D turbulence spreading model *Proceedings of the 41st EPS Conference on Plasma Physics: Europhysics Conference* (Berlin, Germany, 23-27 June 2014)Vol. **38F** P2.067, http://ocs.ciemat.es/EPS2014PAP/pdf/P2.067.pdf

[34] Hariri F. *et al* 2016 *Phys. Plasmas* **23** 052512

[35] Kwon J.M. *et al* 2012 *Nucl. Fusion* **52** 013004

[36] Diamond P.H. *et al* 2013 *Nucl. Fusion* **53** 104019

[37] Lin Y. *et al* 2011 *Nucl. Fusion* **51** 063002

[38] Murakami S. *et al* 2016 *Phys. Plasmas* **23** 012501

[39] Chouli B. *et al* 2014 *Plasma Phys. Control. Fusion* **56** 095018

[40] Chouli1 B. *et al* 2015 *Plasma Phys. Control. Fusion* **57** 125007

[41] Lee H. H. *et al* 2016 *Phys. Plasmas* **23** 082510

[42] Lu Z. X. *et al* 2015 *Phys. Plasmas* **22** 055705

[43] Lu Z.X. *et al* 2015 *Nucl. Fusion* **55** 093012

[44] Shaing K.C. *et al* 2003 *Phys. Plasmas* **10** 1443

[45] Seol J. S. *et al* 2012 *Phys. Rev. Lett.* **109** 195003

[46] Shi Y.J. *et al* 2011 *Phys. Rev. Lett*. **106** 235001

[47] Candy J. and Waltz R. E. 2003 *J. Comput. Phys*. **186** 545

[48] Candy J. and Waltz R. E. 2003 *Phys. Rev. Lett*. **91** 045001

Figure Captions

Fig.1 The waveforms of two identical ECH (shot13906) and OH (shot13904) shots. (a) line-averaged density, (b) core electron temperature, (c) power of ECH and NBI

Fig.2 Temporal evolutions of electron temperature measured at different radii in the ECH (shot 13906) plasma for the first SMBI pulse in fig.1.

Fig.3 2-D electron temperature fluctuation image from ECEI during NLT in the ECH plasma (shot 13906 at Time=2.132s). The time interval for the two image is 0.26 ms. The pattern of temperature increasing area (red colour) is very clearly seen. The black circle represent the approximate location of the q = 1 surface. The blue spot at the q = 1 surface corresponds to the m/n=1 island, which changes its location in time due to the rotation of the island, a general property of the MHD island.

Fig.4 Profiles of macro parameters for ECH (shot 13906 at Time=2s) and OH (shot 13904 at Time = 3s) discharges in fig.1 at same density. (a) electron temperature, (b) ion temperature, (c) toroidal rotation velocity, (d) gradient of electron and ion temperature

Fig.5 The cutoff density for NLT and threshold density for rotation reversal in OH and ECH power scan shots. The normalized effective collisionality (ν_{eff}) at $\rho \sim 0.5$ at cutoff density and threshold density is also plotted in this figure.

Fig.6 Temporal evolutions of core V_ϕ (measured by CES) and line averaged density for OH plasma and ECH plasmas with power scan.

Fig.7 Power spectra of density fluctuations in the ECH and OH plasmas. The time period in this figure is same as fig.2.

Fig.8 The cross-phase spectra of MIR. Here, 5 dispersions for centre channels with respect to channel 9 are overlapped. These channels located at the same poloidal magnetic surface. The distance between each channel is 0.8cm. The poloidal velocity is estimated from the inverse of the slope of a fitted line (green colour) on the dispersion relation. The measurement positions are about $\rho \sim 0.2$ for the ECH plasma and $\rho \sim 0.35$ for the OH plasma.

Fig.9 Energy confinement time v.s. line average density. The data of 800kW ECH plasma is from the ECH heating phase in shot 16478. The low density data ($<1.3\times10^{19}m^{-3}$) of OH plasma is from shot 16471 and high density data ($>1.5\times10^{19}m^{-3}$) of OH plasma is from OH phase of 16478.

Fig.10 Cartoons shows the torque and damping source for intrinsic rotation in KSTAR

Fig.11 Fluctuation power spectrum of T_e at $\rho\sim0.5$. The data of 400kW ECH is obtained from shot 16473. The other data are taken from shot 16475.

Fig.12 Rotation profiles in #16475.

Fig.13 Temporal evolution of core V_ϕ, density, ECH power, and ν_{eff} at $\rho\sim0.5$ in shot 16478.

Fig.14 Profiles of electron temperature at edge region measured by ECE in shot 16478. ECH is injected at 3.0s.

Fig.15 The mode frequency and the growth rate for the OH plasma and the ECH plasma. The experimental parameters for simulation are from fig.4. Positive mode frequency means the

modes in the electron diamagnetic direction and negative mode frequency means the modes in the ion diamagnetic direction. All modes are in electron direction in this simulation.

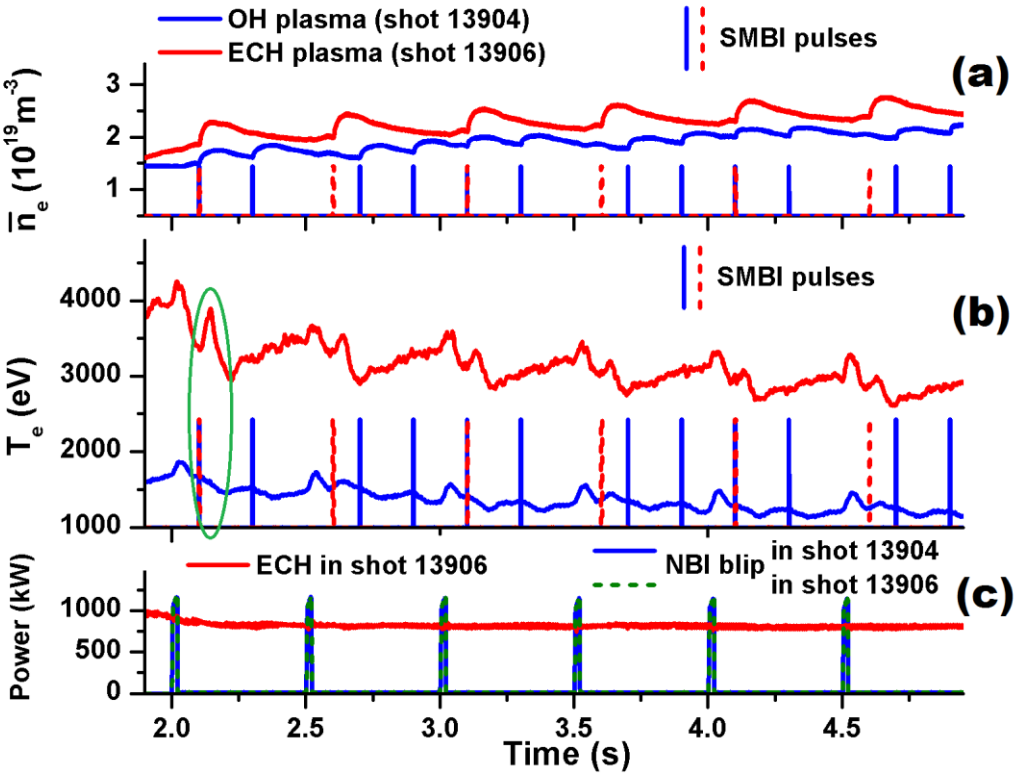

Fig.1 The waveforms of two identical ECH and OH shots. (a) line averaged density, (b) core electron temperature, (c) power of ECH and NBI

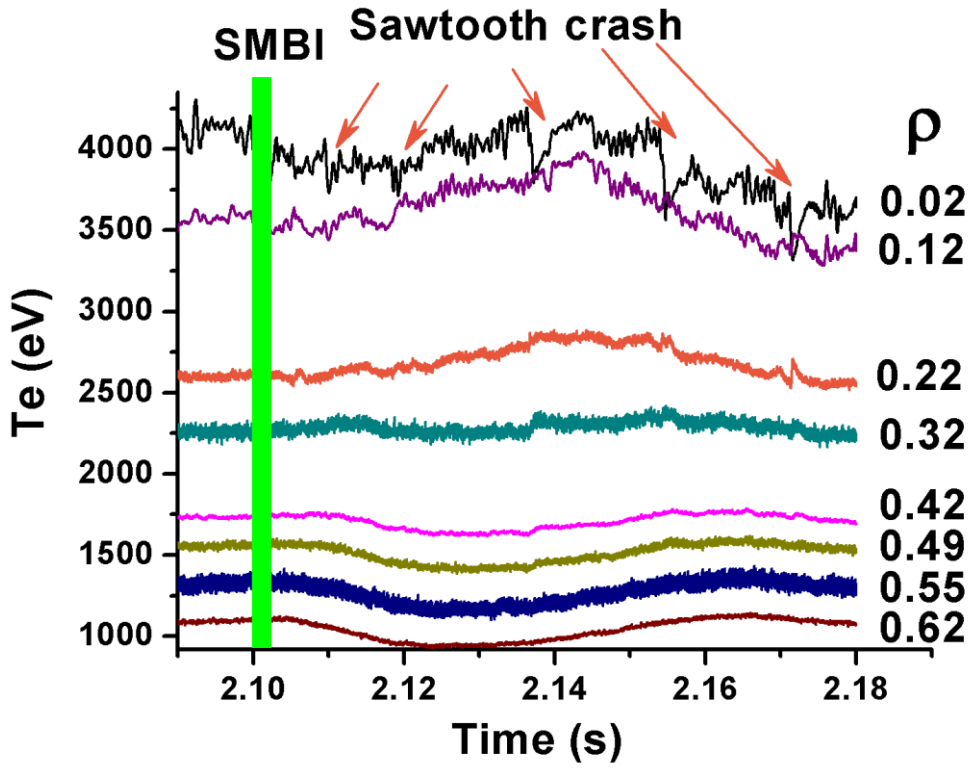

Fig.2 Temporal evolutions of electron temperature measured at different radii in the ECH plasma for the first SMBI pulse in fig.1.

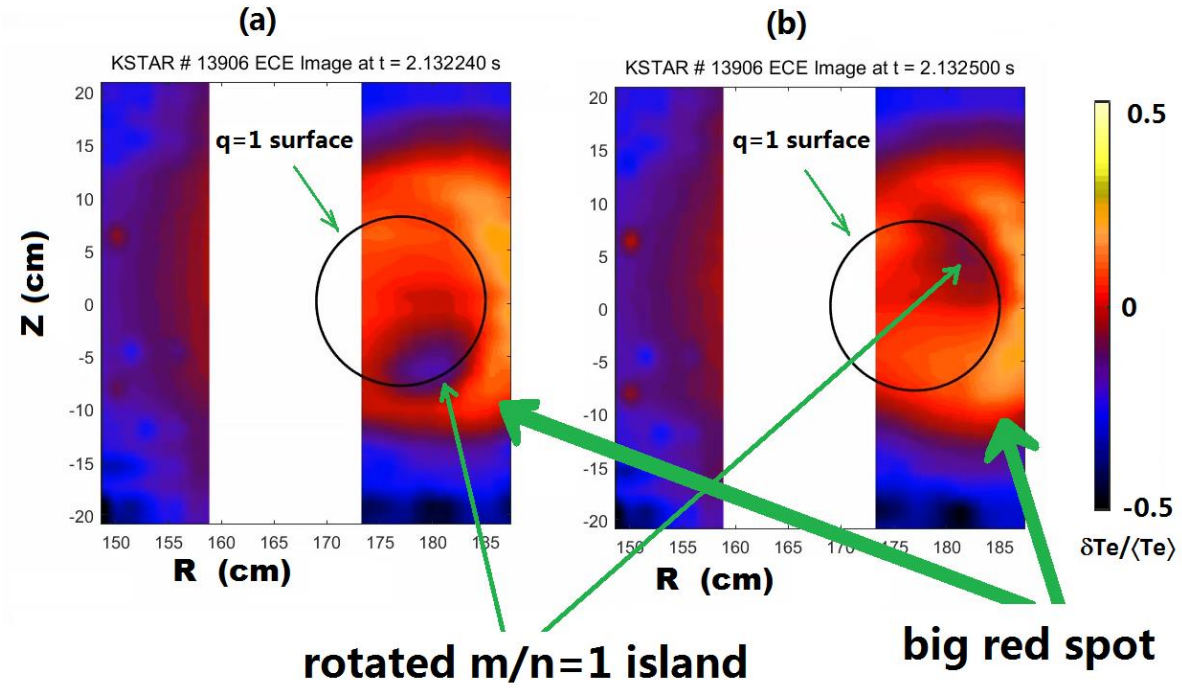

Fig.3 2D electron temperature fluctuation image from ECEI during NLT in ECH plasma (shot 13906). The time interval for the two images is 0.26ms. The pattern of temperature increasing area (red color) is very clear. The black circle represent the approximate location of q=1 surface. The blue spot at the q=1 surface is the m/n=1 island, which is in different location at different time due to the general rotated property of MHD island.

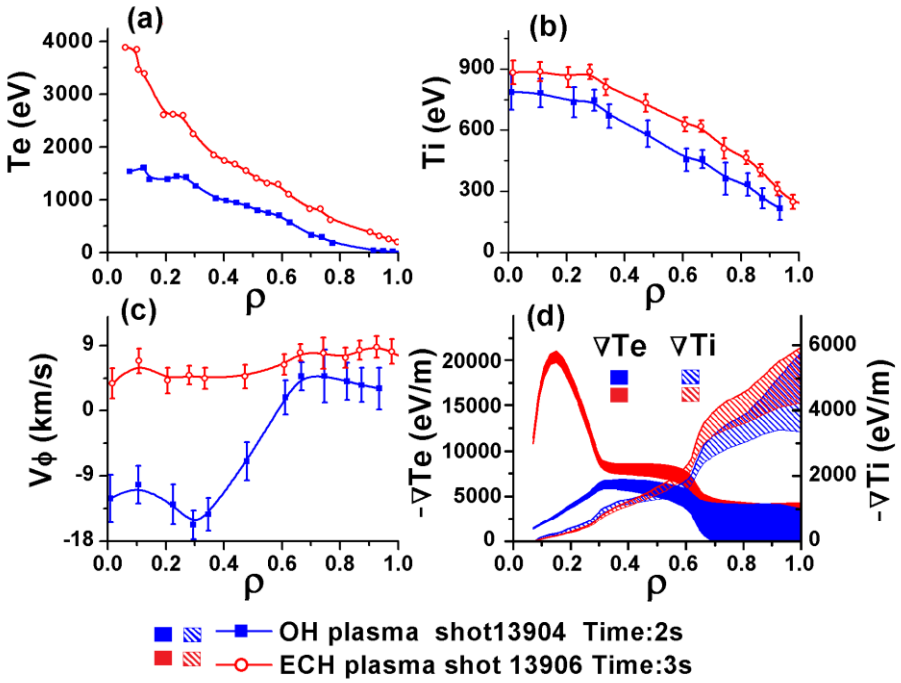

Fig.4 Profiles of macro parameters for two ECH (shot 13906 at Time=2s) and OH (shot 13904 at Time = 3s) discharges in fig.1 at same density. (a) electron temperature, (b) ion temperature, (c) toroidal rotation velocity, (d) gradient of electron and ion temperature

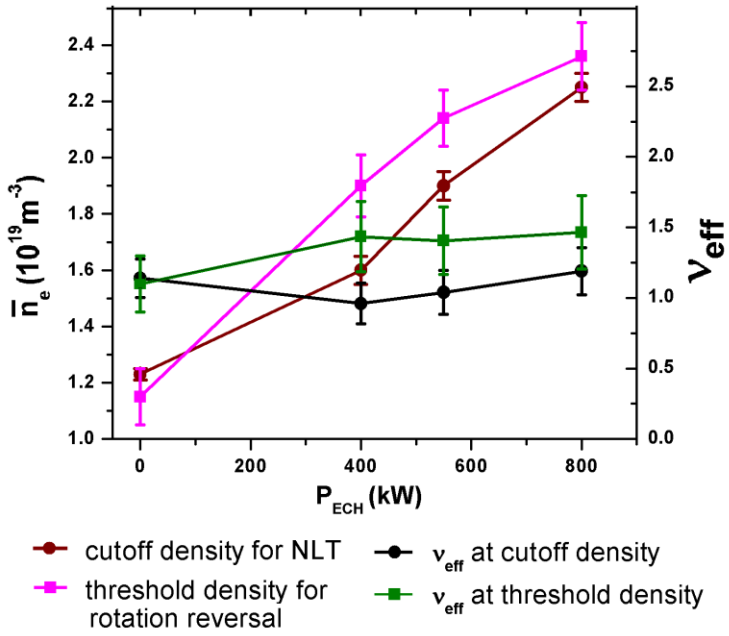

Fig.5 The cutoff density for NLT and threshold density for rotation reversal in ECH power scan shots. The normalized effective collisionality (ν_{eff}) at ρ~0.5 at cutoff density and threshold density is also plotted in this figure.

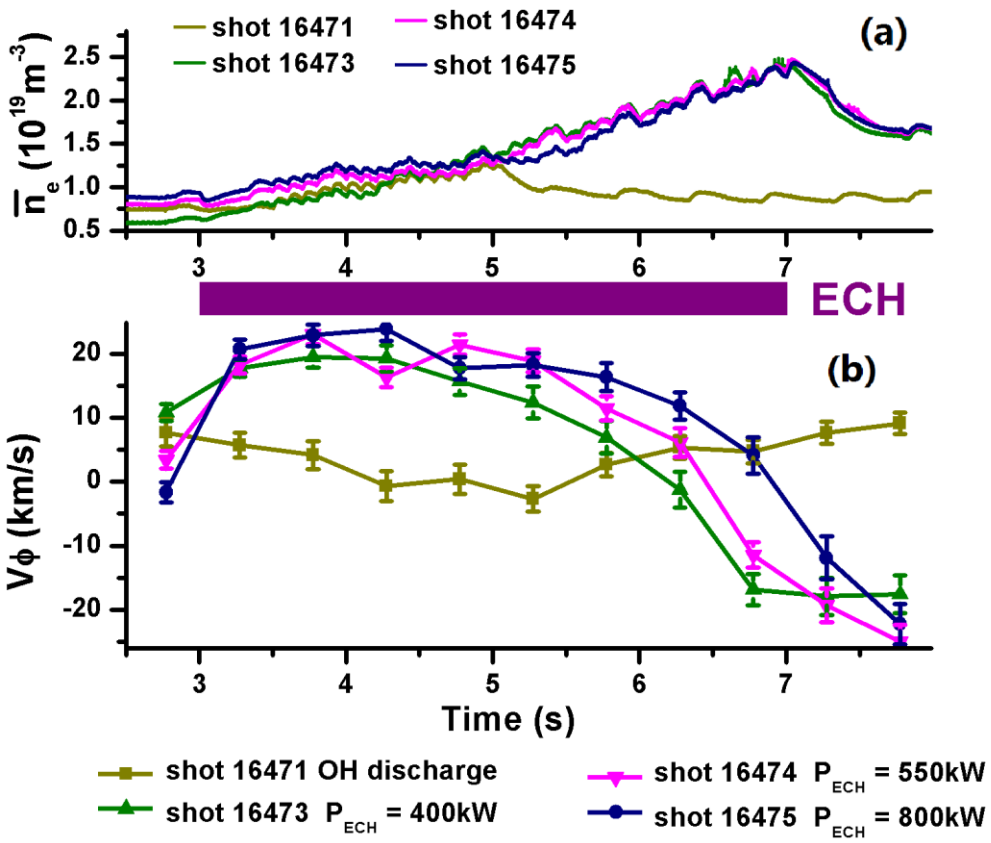

Fig.6 Temporal evolutions of core V_ϕ (measured by CES) and line averaged density for OH plasma and ECH plasmas with power scan.

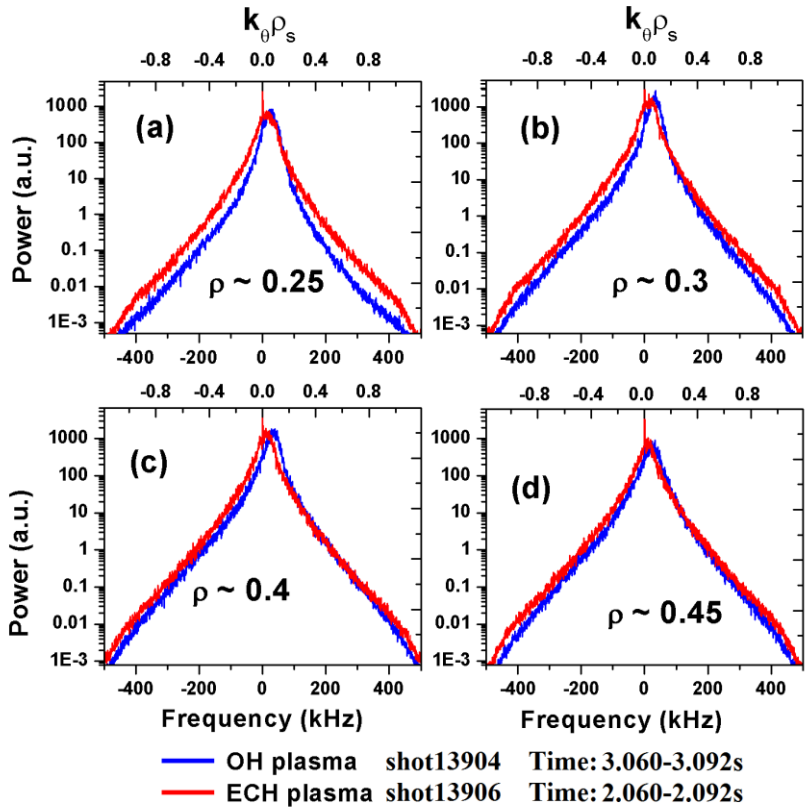

Fig.7 Power spectra of density fluctuations in the ECH and OH plasmas. The time period in this figure is same as fig.4.

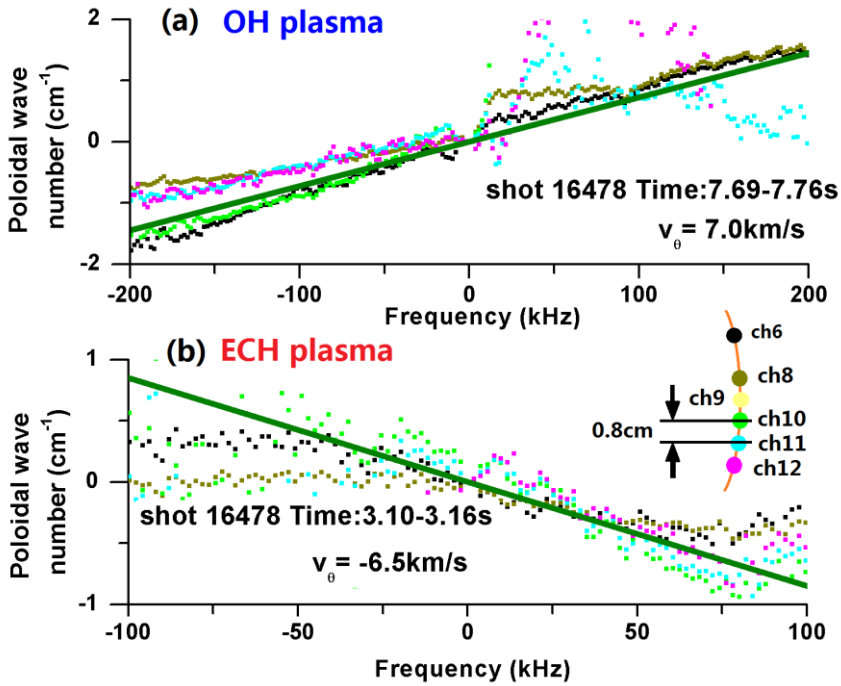

Fig.8 The cross-phase spectra of MIR. Here, 5 dispersions for centre channels with respect to channel 9 are overlapped. The poloidal velocity is estimated from the inverse of the slope of a fitted line (green color) on the dispersion relation. The measurement position is about ρ~0.2 for ECH plasma and ρ~0.35 for OH plasma.

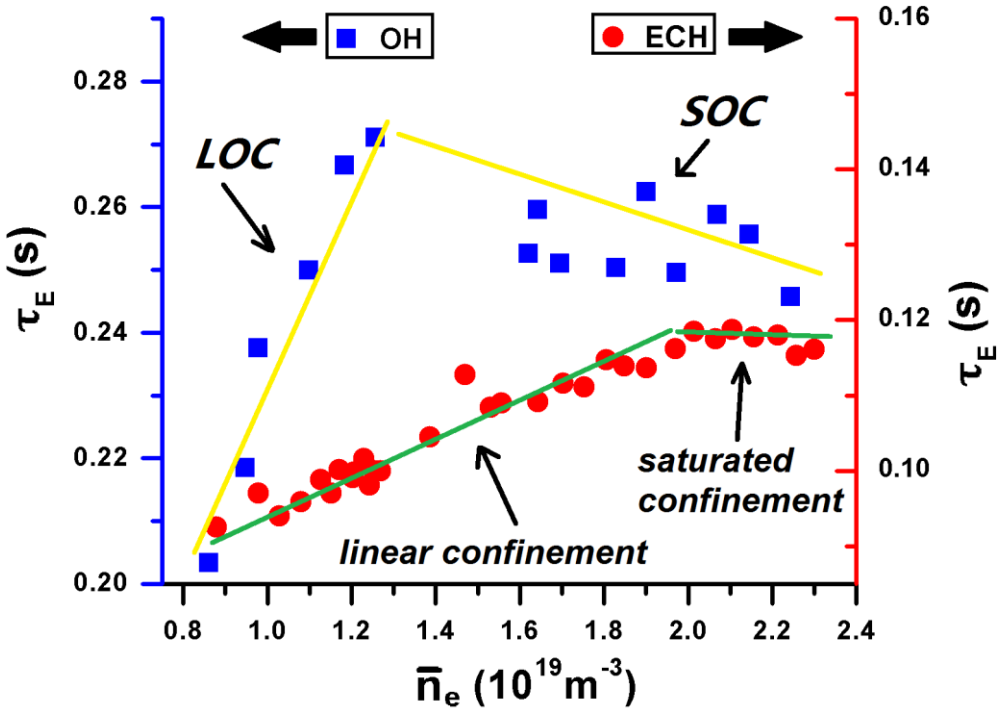

Fig. 9 Energy confinement time v.s. line average density. The data of 800kW ECH plasma is from the ECH heating phase shot 16478. The low density data (<1.3×10^{19}m^{-3}) of OH plasma is from shot 16471 and high density data (>1.5×10^{19}m^{-3}) of OH plasma is from OH phase of 16478.

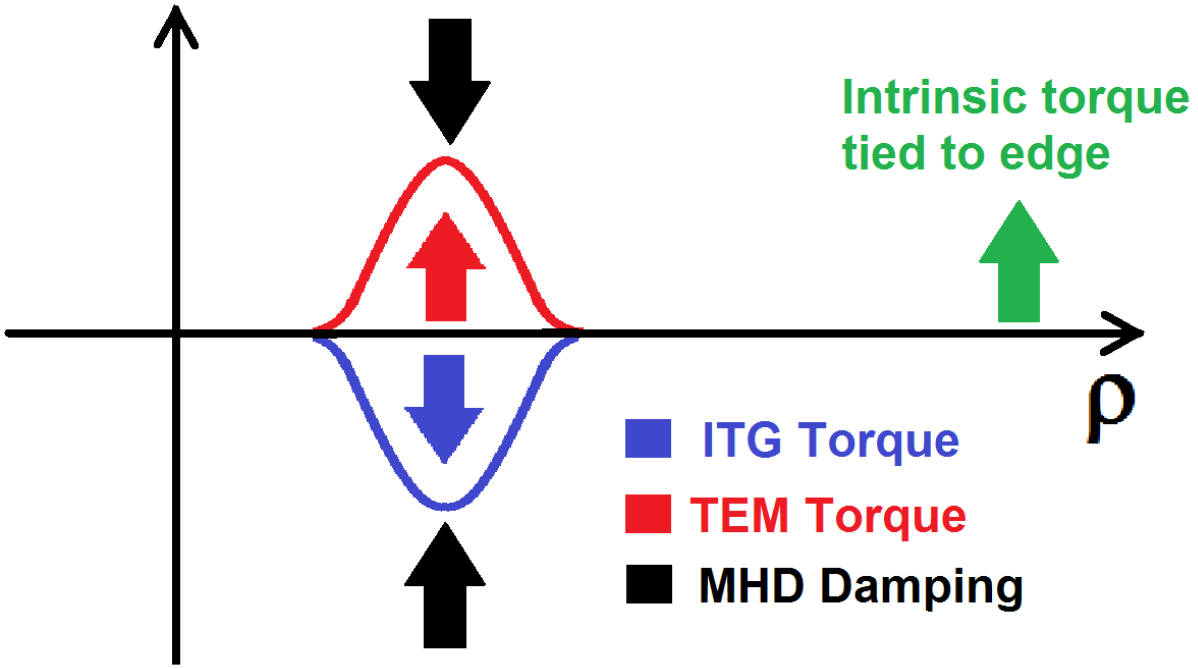

Fig.10 Cartoons shows the torque and damping source for intrinsic rotation in KSTAR

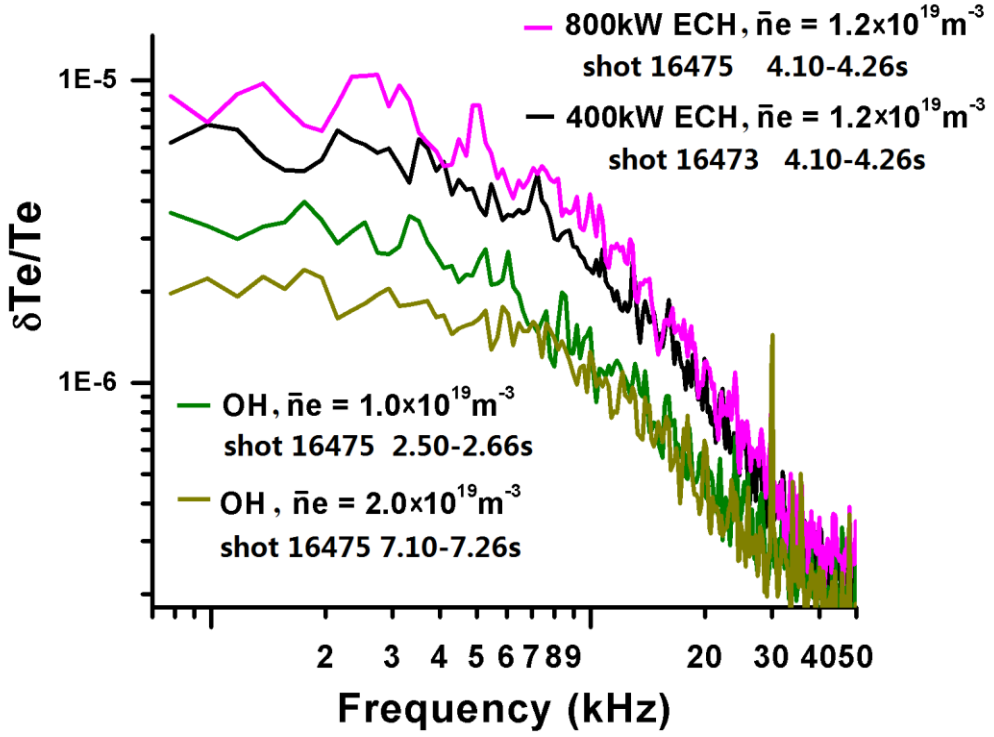

Fig.11 Fluctuation power spectrum of T_e at ρ~0.5. The data of 400kW ECH is obtained from shot 16473. The other data are taken from shot 16475.

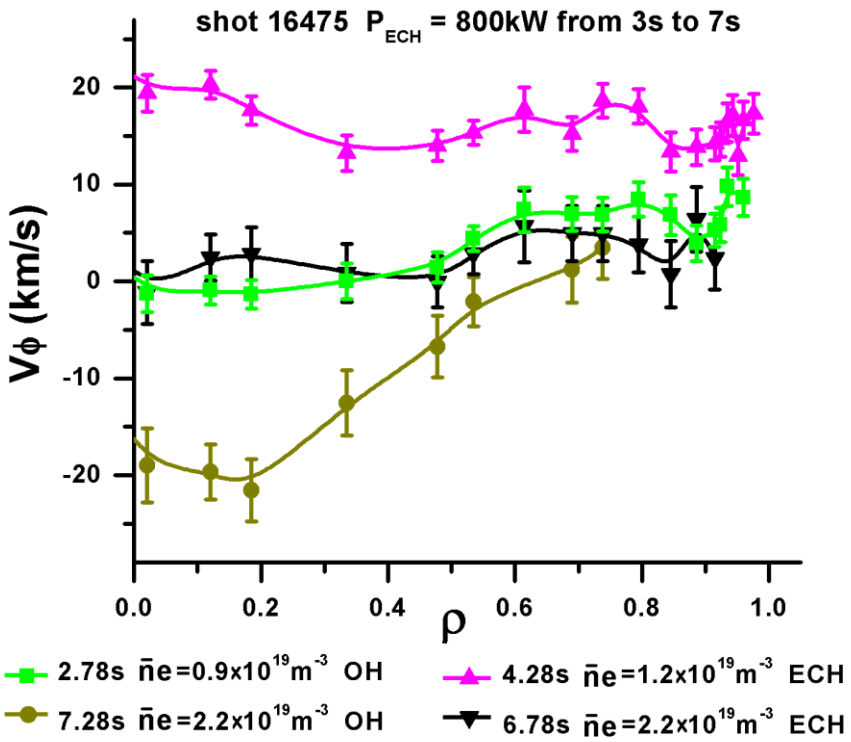

Fig.12 Rotation profiles in shot 16475.

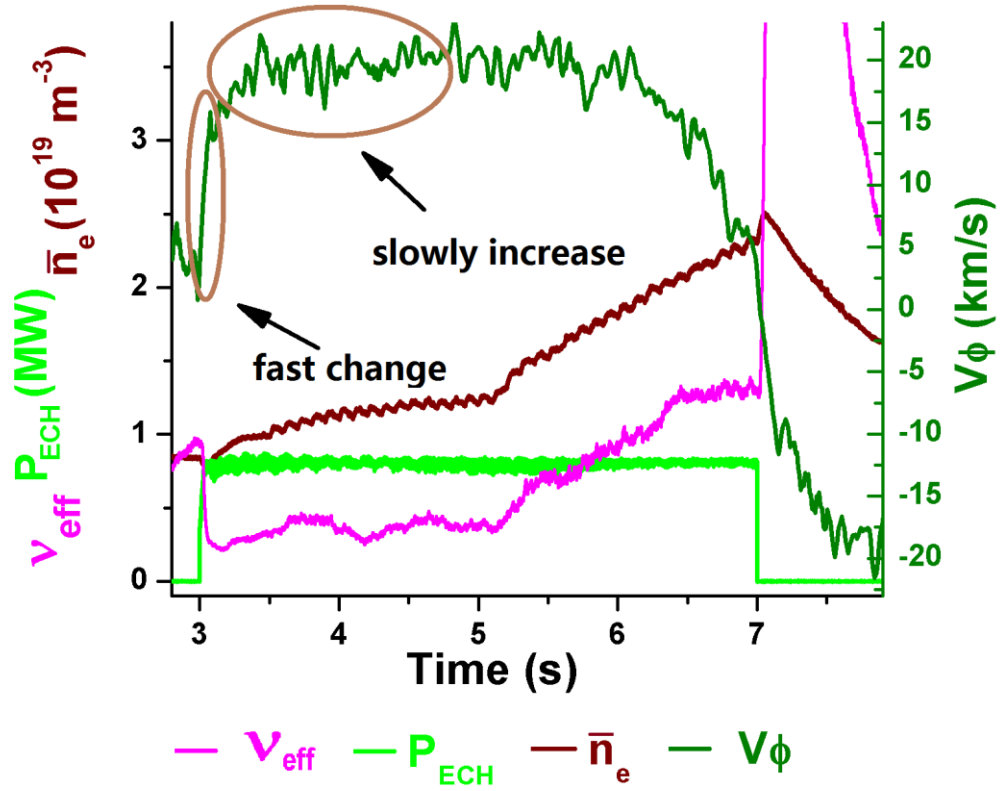

Fig.13 Temporal evolution of core V_ϕ, line averaged density, power of ECH, and ν_{eff} at ρ~0.5 in shot 16478

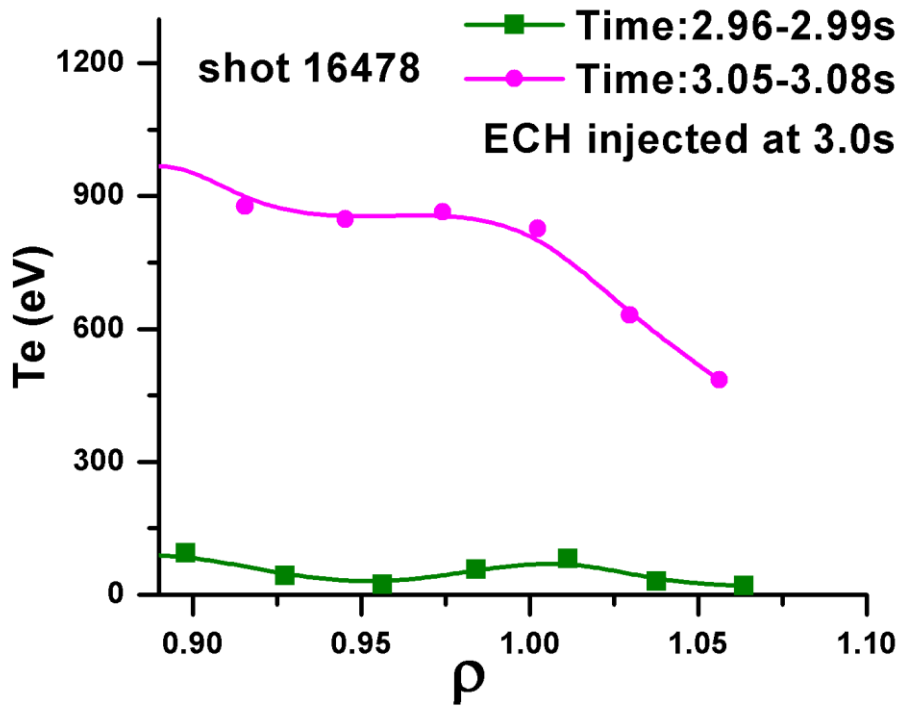

Fig.14 Profiles of electron temperature at edge region in shot 16478. ECH is injected at 3.0s.

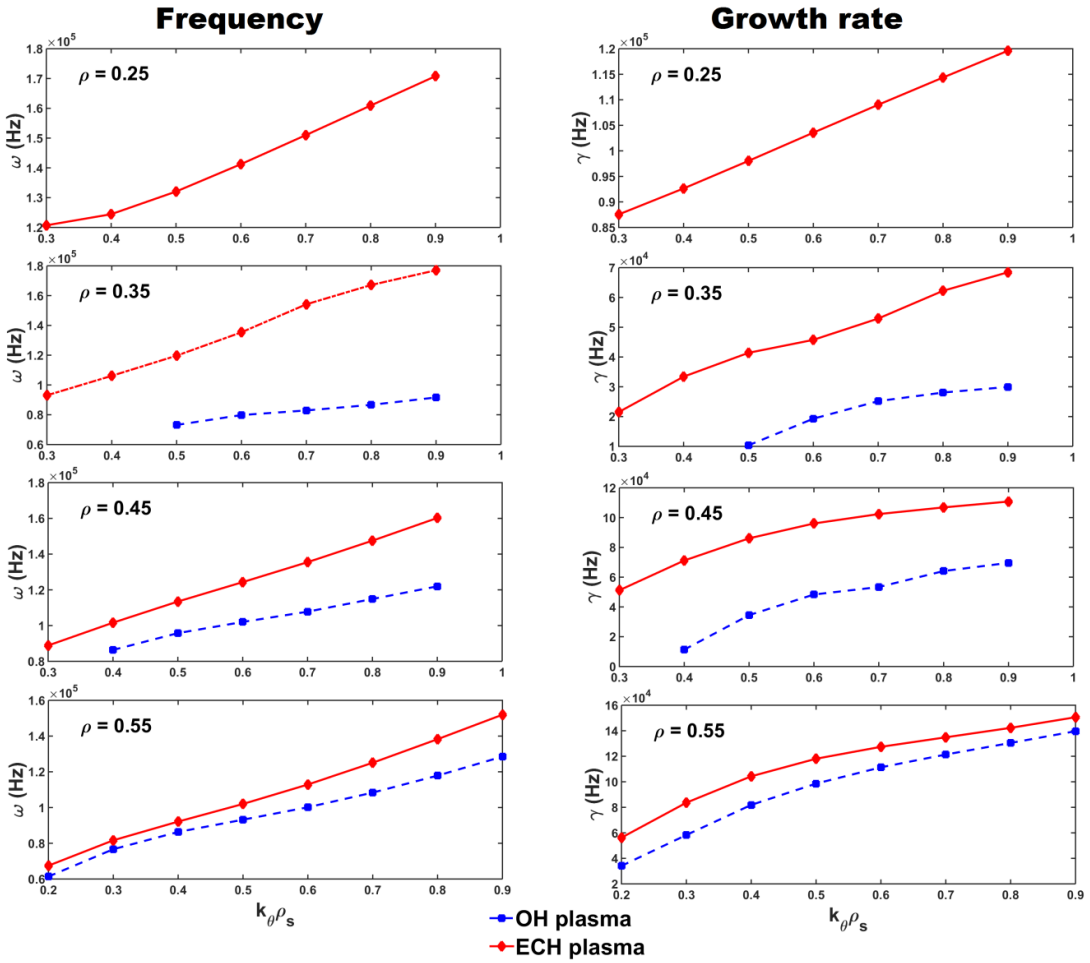

Fig.15 The mode frequency and growth rate for OH plasma and ECH plasma. The experimental parameters for simulation are from fig.4. Positive mode frequency means the modes in the electron diamagnetic direction; negative mode frequency means the modes in the ion diamagnetic direction. All modes are in electron direction in this simulation